
USING SIMULATION OPTIMIZATION TO IMPROVE ZERO-SHOT POLICY TRANSFER OF QUADROTORS

A PREPRINT

Sven Gronauer*, Matthias Kissel, Luca Sacchetto, Mathias Korte and Klaus Diepold

Department of Electrical and Computer Engineering
Technical University of Munich (TUM), Germany
Arcisstr. 21, 80333 Munich

January 6, 2022

ABSTRACT

In this work, we show that it is possible to train low-level control policies with reinforcement learning entirely in simulation and, then, deploy them on a quadrotor robot without using real-world data to fine-tune. To render zero-shot policy transfers feasible, we apply simulation optimization to narrow the reality gap. Our neural network-based policies use only onboard sensor data and run entirely on the embedded drone hardware. In extensive real-world experiments, we compare three different control structures ranging from low-level pulse-width-modulated motor commands to high-level attitude control based on nested proportional-integral-derivative controllers. Our experiments show that low-level controllers trained with reinforcement learning require a more accurate simulation than higher-level control policies.

1 Introduction

Programming intelligent control strategies for complex robot systems is a challenging task. Reinforcement learning (RL) promises the automated synthesis of control strategies through a data-driven approach instead of explicitly designing hand-crafted solutions through expert knowledge. In recent years, the field of RL has witnessed outstanding successes and raised a surge of interest in the control of dynamical systems through such a trial-and-error paradigm. The combination of RL and deep learning methods excel at problems that can be quickly simulated like robotics [13, 22] or video games [18, 29] and in domains where the exact model is known but long-horizon planning is not computationally tractable, e.g. board games like Go and Chess [26].

Despite the significant advances in recent years, the applicability of RL algorithms is still limited when the data at test time differ from those seen during training [10]. Since many real-world systems cannot afford to learn policies from scratch due to the expense of data, simulations are the preferred approach to build data-driven control policies in the RL community. In fact, a gap between the simulation and the real world still persists because the modeling of all effects either requires in-depth expert knowledge or is simply not desirable, e.g. calculating all aero-dynamical effects can significantly increase simulation time. A successful policy transfer thus requires the reality gap to be small.

In this paper, we address the sim-to-real gap in the domain of quadrotor control. Our contributions are threefold:

- We apply simulation optimization as a purely data-driven approach to narrow the reality gap and demonstrate that a zero-shot policy transfer is feasible with minimal expert knowledge. The therefore necessary data were collected for approximately one hour on the real-world quadrotor with a pre-implemented proportional-integral-derivative (PID) controller from the hardware platform.
- We deploy low-level control policies based on pulse-width modulated (PWM) thrust commands trained entirely in simulation on the real-world quadrotor without fine-tuning. To the best of our knowledge, this is the first work using RL that accomplishes successful zero-shot transfers to a real-world quadrotor based on

*Contact author: sven.gronauer@tum.de

low-level control while having access to only onboard sensor values and running all computations on the embedded hardware.

- We study three control structures that differ in their level of abstraction: PWM, attitude rate and attitude control. Through extensive real-world experiments, we investigate the required fidelity of the simulation based on the deployed control structure.

Throughout this work, we focus on the context of zero-shot policy transfer, i.e. we train the agent entirely in simulation and then deploy the policy on a quadrotor robot without using real-world data to fine-tune.

2 Related Work

Quadrotor Control. For attitude control and set-point tracking of quadrotors, a common approach is a hierarchical control that consists of nested PID controllers [16]. Further approaches like linear quadratic regulator are also suitable methods for the stabilization around the hover conditions under reasonably small roll and pitch angles. However, when more dynamic flight behaviors are desired, more complex controllers may be required [17]. Due to their highly dynamic movement capabilities, quadrotors depict an interesting platform to test maneuvers such as landing [11] and perform acrobatic maneuvers like loopings and rolls [9], multi-flips [15] or flying through narrow vertical gaps [17]. While most of these aforementioned works rely on highly accurate state estimation, only a few papers have considered quadrotor control based on lone onboard sensor signals. Lambert et al. [12] used model-based RL to train a policy solely from real-world data while relying only on onboard sensor measurements to run control with direct motor PWM outputs. However, neural network calculations were executed on a server and then transmitted via radio to the drone. They leveraged 180s of real-world flights to produce a controller capable of accomplishing at most 6s of flight time.

Bridging the Reality Gap. To reduce the gap between simulation and real-world, *domain randomization* has been proposed to augment the variability of data by randomization. One way is to randomize the dynamics where simulation parameters responsible for the description of the system transitions are re-sampled at the beginning of every trajectory [21]. Another approach is to randomize the rendering of image-based observations in the simulation [28]. Loquercio et al. [14] showed that agile drone racing is possible with convolutional neural networks when robustly trained on an abundance of image-based data. Another method to narrow the reality gap is *simulation optimization* [1, 27] which is a data-driven approach to identify simulation parameters based on real-world data. Chebotar et al. [2] learned a simulation parameter distribution based on collected data from a physical manipulator robot.

Zero-shot Policy Transfer. In the area of RL, there have been only a few works that study the zero-shot policy transfer to real-world quadrotors. Kaufmann et al. [9] showed that attitude rate control based on image-based and onboard data could perform highly agile maneuvers such as rolls and loopings. Most similar to our work is the work by Molchanov et al. [19] who showed that low-level PWM-based controllers could stabilize and generalize to multiple sizes of quadrotors while entirely being trained in simulation. In contrast to our work, they used an external tracking system to accurately estimate the drone state.

3 Preliminaries

3.1 Reinforcement Learning

A Markov Decision Process (MDP) is formalized by a tuple $(\mathbb{S}, \mathbb{A}, \mathcal{P}, r, \mu)$, where \mathbb{S} and \mathbb{A} denote the state and action space, respectively. $\mathcal{P} : \mathbb{S} \times \mathbb{A} \rightarrow P(\mathbb{S})$ describes the system transition probability, μ denotes the initial state distribution and $r : \mathbb{S} \times \mathbb{A} \rightarrow \mathbb{R}$ is the reward function which we use to incentivize the desired behavior. Let $\tau = (s_0, a_0, s_1, a_1, \dots)$ be a trajectory generated under the policy π with $s_{t+1} \sim \mathcal{P}(\cdot | s_t, a_t)$, $a_t \sim \pi(\cdot | s_t)$ and $s_0 \sim \mu$. The trajectory return is denoted by $R(\tau) = \sum_{t=0}^{\infty} \gamma^t r(s_t, a_t)$. We use the shortcut $\tau \sim \pi$ when trajectories are generated under the policy π . In reinforcement learning, the goal of the agent is to learn a control policy $\pi : \mathbb{S} \rightarrow P(\mathbb{A})$ that maximizes the expected return $J(\pi) = \mathbb{E}_{\tau \sim \pi} [R(\tau)]$ under the infinite horizon with the discount factor $\gamma \in (0, 1)$. In deep RL, the policy π_θ is parametrized by a neural network with the weight vector θ .

In this work, we sample system parameters ξ from a distribution Ξ at the beginning of each trajectory. This results in the system transition probability being dependent on the system parameters $s_{t+1} \sim \mathcal{P}(\cdot | s_t, a_t, \xi)$ which is known as domain randomization. Thus, we seek policy parameters that maximize the expected return

$$\max_{\theta} J(\pi_\theta) = \mathbb{E}_{\xi \sim \Xi} [\mathbb{E}_{\tau \sim \pi_\theta} [R(\tau)]] \quad (1)$$

over the dynamics induced by the distribution of simulation parameters.

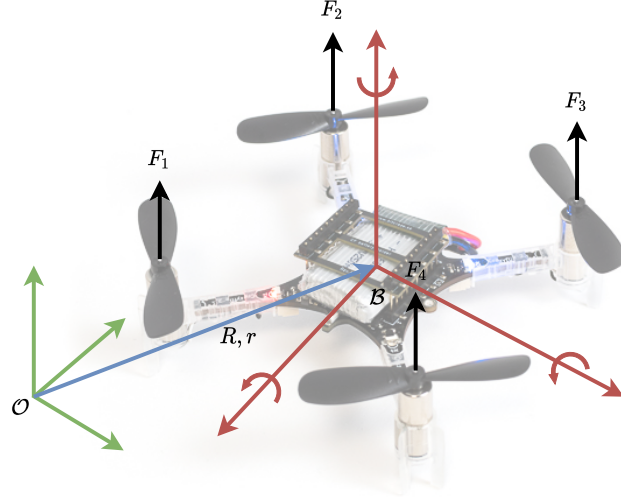


Figure 1: Overview and coordinates frames of the *CrazyFlie* quadrotor.

3.2 Quadrotor

3.2.1 Dynamics Model

The dynamics of the quadrotor are modeled by the differential equation

$$\dot{\mathbf{x}} = f(\mathbf{x}, \mathbf{u}) \quad (2)$$

where the drone state $\mathbf{x} = [\mathbf{r}^T, \dot{\mathbf{r}}^T, \varphi^T, \omega^T]^T \in \mathbb{R}^{13}$ encompasses the position \mathbf{r} , the linear velocity $\dot{\mathbf{r}}$, the body angle φ in quaternions and the angular speed ω . The acceleration of the drone's center of mass is described by Newton's equation

$$m\ddot{\mathbf{r}} = \begin{bmatrix} 0 \\ 0 \\ -mg \end{bmatrix} + R \begin{bmatrix} 0 \\ 0 \\ \sum F_i \end{bmatrix} \quad (3)$$

in the inertial frame \mathcal{O} with gravity g . The quadrotor mass is m and $\sum F_i$ is the sum of the vertical forces acting on the rotors with R being the rotation matrix from the body frame \mathcal{B} to the inertial frame. The angular acceleration governed by Euler's rotation equations in the body frame \mathcal{B} is

$$I\dot{\omega} = \eta - \omega \times (I\omega) \quad (4)$$

with the inertia matrix I . The torques η acting in \mathcal{B} are determined by

$$\eta = \begin{bmatrix} \frac{1}{\sqrt{2}}L(-F_1 - F_2 + F_3 + F_4) \\ \frac{1}{\sqrt{2}}L(-F_1 + F_2 + F_3 - F_4) \\ -M_1 + M_2 - M_3 + M_4 \end{bmatrix} \quad (5)$$

with the rotor forces F_i , the corresponding motor torques M_i and the arm length L . An overview of the quadrotor setup and the coordinate frames is depicted in Figure 1.

3.2.2 Motor Model

The angular speed ν_i of rotor i produces a vertical force

$$F_i = \frac{mg}{4} k_F \nu_i^2 \quad (6)$$

that lifts the quadrotor. We use $k_F \in \mathbb{R}$ to denote the thrust-to-weight ratio. The rotors also produce a moment according to

$$M_i = k_{M_1} F_i + k_{M_2} \quad (7)$$

with k_{M_1} and k_{M_2} being scalars. The motor speeds are normalized $\nu_i \in [0, 1]$ and are modeled $\boldsymbol{\nu} = \sqrt{\mathbf{u}}$ as the square root² of normalized commanded thrusts $u_i \in [0, 1]$. For PWM control, the relationship between the action \mathbf{a} taken by the agent and the normalized commanded thrust is $u_i = \frac{1}{2} [\min(\max(a_i, -1), 1) + 1]$.

We model the motor dynamics with the differential equation of first order

$$T_m \dot{\nu}_i = -\nu_i + \sqrt{u_i}, \quad (8)$$

where $T_m \in \mathbb{R}$ is the motor time constant. A common approach in related work is to neglect the motor dynamics and assume an instantaneous thrust acting on the rotors. However, as we observed in our experiments, an accurate actuator model is crucial for a successful sim-to-real transfer. Additionally, we model the overall latency Δ of the system which should capture all delays emerging on the hardware. Typically, latency arises in the state estimator, in the actuation of the motors and by propagating data through the neural network policy.

4 Methods

We aim to find a policy that reliably transfers from the simulation to the quadrotor robot without using real-world data to fine-tune. To render a zero-shot policy transfer feasible, we search for the optimal parameters with simulation optimization based on collected real-world measurements. The remainder of this section describes the details of our simulation environment including the observation and action space, the procedure of the simulation optimization using Bayesian optimization and an introduction to the three control structures that were deployed and evaluated on the real-world quadrotor.

4.1 Simulation Environment

We use the physics simulator PyBullet [3] to calculate the dynamics of the quadrotor akin to the work of [20]. We run the simulator and the motor dynamics with 200Hz while the agent receives noisy observations with ≤ 100 Hz dependent on the implemented control structure.

Observations. The agent perceives the observation $\mathbf{s}_t = [\mathbf{x}_t^T, \mathbf{e}_t^T, \mathbf{a}_{t-1}^T]^T \in \mathbb{R}^{20}$ containing the drone state vector $\mathbf{x} \in \mathbb{R}^{13}$, the difference vector $\mathbf{e} = \mathbf{r} - \mathbf{t} \in \mathbb{R}^3$ between the drone’s current position and the set-point position and the action $\mathbf{a}_{t-1}^T \in \mathbb{R}^4$ taken previously. Note that the agent cannot access all information of the ground-truth state because the rotor speeds cannot be measured directly. To cope with partial observability, the agent is equipped with a history of observations with size $H \geq 1$, i.e. $(\mathbf{s}_{t-H+1}, \dots, \mathbf{s}_t) \in \mathbb{R}^{20H}$. We conducted a study about the optimal history size $H \in [1, 2, 4, 6, 8]$ in simulation and found that $H = 2$ performed best.

Actions. Actions represent abstract, possibly high-level, commands which are transformed by the control structure to the corresponding motor command $\mathbf{u} \in \mathbb{U}$. The implementation from \mathbb{A} to \mathbb{U} differs for each control structure and is explained in Section 4.3.

Domain Randomization. Throughout training, we randomize the following system parameters uniformly in the range $\pm 10\%$ of the default value: Thrust-to-weight ratio k_F , physics time-step, quadrotor mass m , diagonal of inertia matrix I , motor time constant T_m and yaw-torque factors k_{m_1} and k_{m_2} .

Noise. As sensor noise, we add Gaussian and uniform noise for positions \mathbf{r} , velocities $\dot{\mathbf{r}}$ and angles $\boldsymbol{\varphi}$. For the angle rates, we apply the sensor model proposed in [5] which adds a Gaussian noise and a time-varying bias to $\boldsymbol{\omega}$. In a similar vein to [19], we use a discretized Ornstein–Uhlenbeck process to model actuator noise which we add to \mathbf{u} .

4.2 Simulation Optimization

Simulation optimization is an approach to tune the parameters of a simulation through data [1]. The aim is to bring the simulation as close as possible to the real-world and ideally close the reality gap. The objective function which we want to minimize is

$$\min_{\boldsymbol{\xi} \in \Xi} F(\boldsymbol{\xi}, \mathcal{D}) = \sum_t^T \delta^t \|W(\mathbf{x}_t^{sim}(\boldsymbol{\xi}) - \mathbf{x}_t^{real})\|_1 + \sum_t^T \delta^t \|W(\mathbf{x}_t^{sim}(\boldsymbol{\xi}) - \mathbf{x}_t^{real})\|_2 \quad (9)$$

²The CrazyFlie firmware internally uses a quadratic model that considers battery level and the commanded thrust $\mathbf{u} \in [0, 1]$ and maps it to the corresponding PWM value.

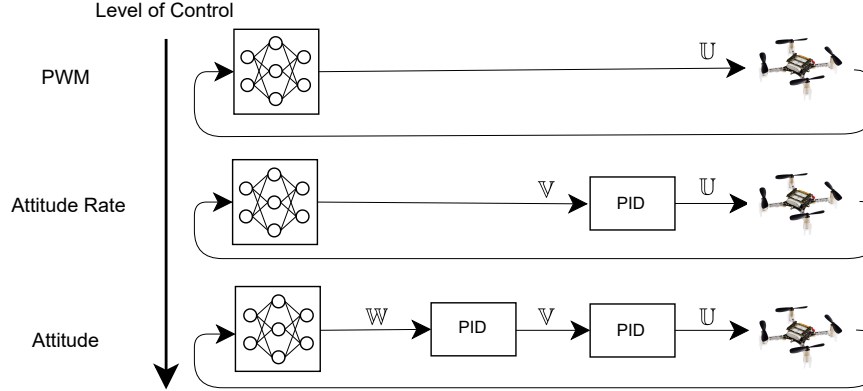


Figure 2: Control structures from low to high level. (1) *PWM*: A neural network-based policy directly outputs the commanded thrusts. (2) *Attitude Rate*: The policy commands the desired angle rates and collective thrust which are subsequently fed into a PID controller. (3) *Attitude*: The cascaded PID controllers take the desired body angle and collective thrust as input and output the commanded thrusts for each motor.

where T is the mini-trajectory length, \mathcal{D} is the data set and $\delta \in (0, 1)$ is a factor to discount later stages of the trajectory where the divergence increases due to discrepancies between simulation and real-world. We weight the drone state difference $\mathbf{x}_t^{sim}(\xi) - \mathbf{x}_t^{real}$ according to the matrix W with the purpose to scale angle errors and angle rate errors differently. Similar to [2], we use the sum of both L1 and L2 norm.

Prior sim-to-real work reported that the accurate modeling of the actuators including dynamics, noise and delays is crucial for a successful transfer. Peng et al. [21] pointed out that randomizing the latency of the controller and injecting sensor noise to the simulation are key components for a high success rate. Similarly, Hwangbo et al. [8] demonstrated that learned actuator dynamics significantly helped to reduce the reality gap. Guided by these results, we decided to find the optimal simulation parameters $\xi = [k_F, T_m, \Delta]^T$ that describe the motor behavior as well as the latency.

We chose Bayesian Optimization (BO) as method since it is regarded as a good choice for the optimization over continuous domains with less than 20 dimensions while being robust to stochastic function evaluations [4]. BO is particularly suited for objective functions that have long evaluation times and, thus, require low sample complexity. In contrast to gradient-based methods, BO is not prone to converge to local optima and is able to find a global solution.

4.3 Control Structures

We hypothesize that low-level control structures require a higher simulation fidelity. Low-level control requires the policy to learn the underlying dynamics of the quadrotor to exert full control over the robot. High-level control, on the other hand, encourages the agent to learn an abstract understanding of the task while the nested PID controllers handle the underlying drone dynamics. In this work, we investigate the following three control structures, ordered from low to high-level.

1. *PWM Control*. The agent is supposed to learn a mapping $\pi : \mathcal{S} \rightarrow \mathcal{U}$ from observation space to thrust commands. The agent receives noisy observations from the Kalman state estimator with 100Hz.
2. *Attitude Rate Control*. The policy output lies in the space $[c, \omega_d^T]^T \in \mathcal{V} \subseteq \mathbb{R}^4$ which consists of the mass-normalized collective thrust c and the desired body angle rate ω_d . The PID controller calculates the thrust commands $\mathbf{u} \in \mathcal{U}$ based on c and the error between actual ω and desired body angle rate ω_d . The agent receives noisy observations with 50Hz and is supposed to learn the mapping $\pi : \mathcal{S} \rightarrow \mathcal{V}$.
3. *Attitude Control*. The agent is incentivized to learn the policy $\pi : \mathcal{S} \rightarrow \mathcal{W}$ where the control space $[c, \varphi_d^T] \in \mathcal{W} \subseteq \mathbb{R}^4$ encompasses the mass-normalized collective thrust c and the desired body angle φ_d . Subsequently, the mapping $\mathcal{W} \rightarrow \mathcal{V} \rightarrow \mathcal{U}$ is handled by two cascaded PID controllers. Noisy observations are fed into the policy with 25Hz.

These three control structures are depicted in Figure 2. We test our hypothesis about the fidelity of the simulator based on the employed control method in the next section.

Table 1: Simulation optimization results found by Bayesian Optimization. The mean and given standard deviation was calculated over three trials.

Parameter	$T = 10$	$T = 20$	$T = 30$	$T = 40$	$T = 50$
Thrust-weight k_F	1.746 ± 0.0050	1.733 ± 0.0093	1.725 ± 0.0018	1.725 ± 0.0081	1.722 ± 0.0027
Time Constant T_m	0.102 ± 0.0110	0.087 ± 0.0087	0.088 ± 0.0006	0.096 ± 0.0035	0.104 ± 0.0012
Latency Δ	0.006 ± 0.0039	0.014 ± 0.0038	0.018 ± 0.0003	0.018 ± 0.0007	0.018 ± 0.0004

5 Results

In this section, we describe our experiments and discuss the results. First, we describe the setup of the hardware and the learning task. Second, we elaborate on our simulation optimization experiments with Bayesian optimization and present our found simulation parameters. Third and last, we explain our zero-shot transfer experiments that were conducted on the real-world quadrotor. After training control policies in simulation, we studied the three control structures PWM, attitude rate and attitude in order to test our control level hypothesis.

5.1 Experimental Setup

As quadrotor robot, we used the *CrazyFlie 2.1*³. Due to its small size with a motor-to-motor diameter of 13cm and light weight of 28g, the *CrazyFlie* drone is very agile and demands high control frequencies. Further, due to its low-cost design, the *CrazyFlie* exhibits high parameter uncertainties in its building parts which additionally requires the controller to be robust over a large system parameter distribution. The drone is equipped with a 3-axis gyroscope, a 3-axis accelerometer and a z-axis LIDAR. The sensor values are fed into an extended Kalman filter that runs with 100Hz for drone state estimation. For our experiments, we only used onboard sensor measurements and did not use any external tracking system. For evaluation purposes, we transmitted the flight information via *CrazyRadio* to a host computer where we analyzed the logged data.

As learning task, we want the quadrotor to fly a circle figure with a diameter of 0.5m and a period of 3s. Each trajectory starts on a random point of the reference circle at height 1m going in clock-wise direction. The trajectory length in simulation is 500, which is equivalent to 5s of real-world time. To incentivize the drone following the set-point trajectory \mathbf{t} , the reward function is designed as

$$r(\mathbf{s}, \mathbf{a}, \mathbf{t}) = \|\mathbf{e}\|_2 + 0.0001\|\mathbf{a}_t\|_2 + 0.001\|\mathbf{a}_{t-1} - \mathbf{a}_t\|_2 + 0.001\|\boldsymbol{\omega}\|_2 + r_f \quad (10)$$

with $r_f = -100$ being the terminal reward if $\|\mathbf{e}\|_2 > 0.25$ else $r_f = 0$.

5.2 Simulation Optimization

We used the pre-implemented cascaded PID position controller from the *CrazyFlie Firmware* to collect data tuples $\mathcal{D} = \langle \mathbf{x}, \mathbf{u} \rangle_t$ while the drone is flying the circle figure as described in Section 5.1. Data were logged with 100Hz and we collected approximately one hour of real-world data. For building the data set, we used every tenth data-point as starting state for a mini-trajectories of length T . For instance, for $T = 50$ we obtained a data set of size $\mathcal{D} \in \mathbb{R}^{37673 \times 50 \times 13}$.

With BO, we opted to find the global optimum over the bounded set of system parameters $k_F \in [1.5, 2.5]$, $T_m \in [0.01, 0.50]$ and $\Delta \in [0.00, 0.05]$ based on the real-world measurements \mathcal{D} . We ran the experiment for 250 evaluations on the objective from Eq. 9 and averaged the results over three trials. We tested different mini-trajectory lengths $T \in \{10, 20, 30, 40, 50\}$. As hyper-parameters, we used $\delta = 0.95$ as the discount factor and as function approximator we used a Gaussian process with the acquisition function uniformly chosen from lower confidence bound, expected improvement and probability of improvement.

The results obtained by the simulation optimization are shown in Table 1. Surprisingly and contrary to our expectations, the mini-trajectory length T had only a minor impact on the obtained results. Except for the results with latency $T=10$, the found parameters ξ lie in a similar range despite the different mini-trajectory lengths.

5.3 Zero-Shot Experiments

To evaluate the parameters found by the simulation optimization as well as to test our control level hypothesis, we conducted zero-shot experiments on the real quadrotor. We first trained policy networks with different simulation parameters and thereafter measured the transfer performance.

³<https://www.bitcraze.io/products/crazyflie-2-1/>

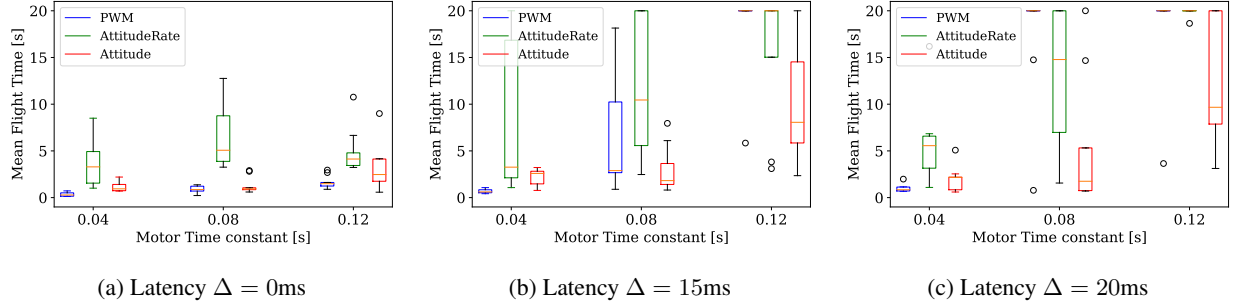


Figure 3: Measured flight times in the zero-shot experiments evaluated for different system parameters and control structures. Each box represents nine real-world flights with a maximum flight time of 20s after which we manually stopped the policy execution.

5.3.1 Training with RL

We aligned the hyper-parameters to the ones suggested in [6, 7] and provide a summary in Table 3 of the Appendix. We applied a distributed learner setup where the policy gradients were computed and averaged across 64 workers with a batch size of 64000. We trained with the PPO algorithm [24] over 500 epochs and applied the discount factor $\gamma = 0.99$. As neural network architecture, we used multi-layer perceptrons with two hidden layers. The critic network used 64 neurons each followed by tanh non-linearities whereas the actor had 50 neurons in each hidden layer with ReLU as activations. Since the policy networks are supposed to run on the drone micro-controller, we reduced the number of hidden neurons to achieve an inference time of < 1 ms for one forward pass. The weights were initialized with Kaiming Uniform and biases were set to zero vectors. We did not apply parameter sharing between the actor and the critic. Both networks were optimized with Adam with the learning rate 0.001 for the value network and 0.0003 for the policy. To reduce the variance of critic estimates, we applied Generalized Advantage Estimation (GAE) [23] with the weighting factor $\lambda = 0.95$. Over the training, we used stochastic policies where the policy output is the mean of a multi-variate Gaussian distribution $\mathbf{a} \sim \mathcal{N}(\pi(\mathbf{s}), \epsilon \mathbb{1})$ with $\mathbb{1}$ being the identity matrix and $\epsilon \in \mathbb{R}$ the exploration noise that was linearly annealed from 0.5 to 0.01.

Based on the parameters found by the simulation optimization, we trained policies in simulation with a thrust-to-weight ratio of $k_F = 1.8$, the motor time constants $T_m \in \{0.04, 0.08, 0.12\}$ and latency $\Delta \in \{0, 15, 20\}$ ms. We decided on such experimental setup for three reasons. First, we wanted to evaluate the performance of the found parameters for an induced reality gap. Second, we intended to study the robustness of the trained policies in different scenarios. Third and last, we wanted to test our control level hypothesis stated in Section 4.3.

5.3.2 Zero-shot Transfers

After the training in simulation, we tested each combination of motor time constant $T_m \in \{0.04, 0.08, 0.12\}$ s and latency $\Delta \in \{0.015, 0.02\}$ s with three different policies and evaluated each policy over three flights. This resulted in $3^4 = 81$ trained neural networks and overall 243 real-world flights. If a policy was able to fly longer than 20s, we manually stopped the execution of the neural network. If the policy was not able to stabilize the quadrotor, the flight was terminated by a stabilizing backup PID controller, which intervened when the roll or pitch angle was greater than 30deg or when roll and pitch rates exceeded 800deg/s. We observed that the rollouts also failed when the distance between the drone and the set-point exceeded the episode termination criterion of $\|e\|_2 > 0.25$ m. The results are displayed in Figure 3.

The PWM control structure showed good zero-shot performance when trained on the motor time constant $T_m = 120$ ms with latency $\Delta \geq 15$ ms. The parameter setting $T_m = 80$ ms, $\Delta = 20$ ms closest to the parameters suggested by the simulation optimization resulted in a median flight time of 20s and two outlier flights. However, outside this parameter setting, PWM fastly dropped in performance and often failed. When the latency was set to $\Delta = 0$ ms, PWM yielded the worst performance compared to the other two control approaches.

Overall, the attitude rate control structure showed the most robust results over the tested system parameters. The best performance was observed for the setting $T_m = 120$ ms and $\Delta = 20$ ms. In contrast to the other control structures, attitude rate was also able to stabilize the quadrotor when trained on latency $\Delta = 0$ ms, although most flights terminated early due to the $\|e\|_2 > 0.25$ m criterion.

Surprisingly, attitude control showed the worst performance despite being the highest control level structure. Only the policies that were trained on settings with $T_m = 120\text{ms}$ and latency $\Delta \geq 15\text{ms}$ could achieve a flight duration over 10s.

6 Discussion

In this section, we discuss our results from the experiments and draw connections to related work. Further, we point out important observations that we made during our experiments.

Simulation Optimization. The system parameters closest to the ones found by the simulation optimization showed a reasonable transfer success for the PWM and attitude rate control. This underlines the potential of data-driven parameter estimation compared to classical methods known from system identification. A benefit is the ease of use since a handful of system parameters can be estimated simultaneously and no isolated measurements of building parts must be run.

Control-level Hypothesis. For low-level PWM control, we found that good zero-shot performance can only be achieved when the dynamics of the actuator and the latency are accurately estimated. However, if the reality gap is too large, low-level policy control is prone to fail. The higher-level attitude rate control, in contrast, shows high robustness towards the choice of system parameters. This confirms our hypothesis from Section 4.3 that low-level control requires higher simulation fidelity than higher-level control structures. Merely attitude control showed disappointing results in the zero-shot experiments, which we think is due to the small control frequency of 25Hz.

Actuator Model. Related work from quadrupedal robots [8] and robotic manipulators [21] suggested that accurate modeling of the actuators is a crucial component for reliable zero-shot policy transfers. Our experiments confirmed that this statement is also valid for quadrotor robots. In addition to that, we observed that adding latency to the simulation acts as a kind of regularization which helped to improve the zero-shot results.

Robustness. Due to crashes and its low-budget design, the *CrazyFlie* drone frequently required the change of spare parts like propellers and motors. Despite the variety of drone parameters, the zero-shot transfers worked reliably. Moreover, we tested the trained policies also on other *CrazyFlie* drones which showed the same flight behavior. This indicates that the trained policies are robust over a large parameter distribution and drone systems as long as the actuators are modeled accurately.

Bang-bang behavior. Bang-bang behavior is a known issue in RL where policies prefer an action selection towards the boundaries of the action space [25]. Without adding penalties to the actions, we observed that agents produced high changes in the control inputs to the real-world quadrotor which caused a severe performance drop in the transfers. By adding penalties for actions $\|\mathbf{a}_t\|_2$ and action rates $\|\mathbf{a}_{t-1} - \mathbf{a}_t\|_2$, we were able to conduct reliable transfers to the real robot. Similar conclusions were made in sim-to-sim experiments where penalties for action and action rate improved both the transfer and the robustness towards disturbances [25]. Further, we noticed that the transfers failed when the action range was selected too high, e.g. an attitude rate control with the range $[-360, 360]\text{deg/s}$ did not work whereas the range $[-60, 60]\text{deg/s}$ showed the desired results.

7 CONCLUSIONS

In this paper, we demonstrated that low-level control policies trained with reinforcement learning entirely in simulation can be directly transferred to a quadrotor robot without using real-world data to fine-tune. Our neural network-based policies used only onboard sensor data for inference and ran on the embedded micro-controller of the drone. To render such zero-shot policy transfers feasible, we collected real-world data with a pre-implemented PID controller and applied simulation optimization to narrow the sim-to-real gap. Finally, we conducted extensive real-world experiments and compared three different control structures ranging from low-level pulse-width-modulated motor commands to high-level attitude control based on cascaded PID controllers.

ACKNOWLEDGMENT

The project on which this report is based was supported by the German Federal Ministry of Education and Research under grant number 01IS17049. The author is responsible for the content of this publication. Further, we want to thank Matthias Emde for his support in the implementation of drone firmware.

References

- [1] Y. Carson and A. Maria, “Simulation optimization: Methods and applications,” in *Proceedings of the 29th Conference on Winter Simulation*, ser. WSC ’97. USA: IEEE Computer Society, 1997, pp. 118–126. [Online]. Available: <https://doi.org/10.1145/268437.268460>
- [2] Y. Chebotar, A. Handa, V. Makoviychuk, M. Macklin, J. Issac, N. Ratliff, and D. Fox, “Closing the sim-to-real loop: Adapting simulation randomization with real world experience,” in *2019 International Conference on Robotics and Automation (ICRA)*, 2019, pp. 8973–8979.
- [3] E. Coumans and Y. Bai, “Pybullet, a python module for physics simulation for games, robotics and machine learning,” <http://pybullet.org>, 2016–2021, accessed: 2021-12-19.
- [4] P. I. Frazier, “A tutorial on bayesian optimization,” *CoRR*, vol. abs/1807.02811, 2018.
- [5] F. Furrer, M. Burri, M. Achtelik, and R. Siegwart, *RotorS—A Modular Gazebo MAV Simulator Framework*. Cham: Springer International Publishing, 2016, pp. 595–625.
- [6] S. Gronauer, M. Gottwald, and K. Diepold, “The successful ingredients of policy gradient algorithms,” in *Proceedings of the Thirtieth International Joint Conference on Artificial Intelligence, IJCAI-21*. International Joint Conferences on Artificial Intelligence Organization, 8 2021, pp. 2455–2461, main Track.
- [7] P. Henderson, R. Islam, P. Bachman, J. Pineau, D. Precup, and D. Meger, “Deep reinforcement learning that matters,” in *Proceedings of the Thirty-Second AAAI Conference on Artificial Intelligence*. AAAI Press, 2018, pp. 3207–3214.
- [8] J. Hwangbo, J. Lee, A. Dosovitskiy, D. Bellicoso, V. Tsounis, V. Koltun, and M. Hutter, “Learning agile and dynamic motor skills for legged robots,” *Science Robotics*, vol. 4, 2019.
- [9] E. Kaufmann, A. Loquercio, R. Ranftl, M. Müller, V. Koltun, and D. Scaramuzza, “Deep drone acrobatics,” in *Proceedings of Robotics: Science and Systems*, Corvallis, Oregon, USA, July 2020.
- [10] R. Kirk, A. Zhang, E. Grefenstette, and T. Rocktäschel, “A survey of generalisation in deep reinforcement learning,” *CoRR*, vol. abs/2111.09794, 2021.
- [11] J. E. Kooi and R. Babuska, “Inclined quadrotor landing using deep reinforcement learning,” in *IEEE/RSJ International Conference on Intelligent Robots and Systems, IROS 2021, Prague, Czech Republic, September 27 - Oct. 1, 2021*. IEEE, 2021, pp. 2361–2368.
- [12] N. O. Lambert, D. S. Drew, J. Yaconelli, S. Levine, R. Calandra, and K. S. J. Pister, “Low-level control of a quadrotor with deep model-based reinforcement learning,” *IEEE Robotics and Automation Letters*, vol. 4, no. 4, pp. 4224–4230, 2019.
- [13] T. P. Lillicrap, J. J. Hunt, A. Pritzel, N. Heess, T. Erez, Y. Tassa, D. Silver, and D. Wierstra, “Continuous control with deep reinforcement learning,” in *4th International Conference on Learning Representations, ICLR 2016, San Juan, Puerto Rico, May 2-4, 2016, Conference Track Proceedings*, Y. Bengio and Y. LeCun, Eds., 2016.
- [14] A. Loquercio, E. Kaufmann, R. Ranftl, A. Dosovitskiy, V. Koltun, and D. Scaramuzza, “Deep drone racing: From simulation to reality with domain randomization,” *IEEE Transactions on Robotics*, 2019.
- [15] S. Lupashin, A. Schöllig, M. Sherback, and R. D’Andrea, “A simple learning strategy for high-speed quadcopter multi-flips,” in *Proceedings of the IEEE International Conference on Robotics and Automation (ICRA) 2010, Zurich, 2009, 2010 IEEE International Conference on Robotics and Automation; Conference Location: Anchorage, AK, USA; Conference Date: May 3-8, 2010*.
- [16] R. Mahony, V. Kumar, and P. Corke, “Multirotor aerial vehicles: Modeling, estimation, and control of quadrotor,” *IEEE Robotics Automation Magazine*, vol. 19, no. 3, pp. 20–32, 2012.
- [17] D. Mellinger and V. Kumar, “Minimum snap trajectory generation and control for quadrotors,” in *2011 IEEE International Conference on Robotics and Automation*, 2011, pp. 2520–2525.
- [18] V. Mnih, K. Kavukcuoglu, D. Silver, A. A. Rusu, J. Veness, M. G. Bellemare, A. Graves, M. Riedmiller, A. K. Fidjeland, G. Ostrovski, S. Petersen, C. Beattie, A. Sadik, I. Antonoglou, H. King, D. Kumaran, D. Wierstra, S. Legg, and D. Hassabis, “Human-level control through deep reinforcement learning,” *Nature*, vol. 518, pp. 529 EP –, 02 2015. [Online]. Available: <https://doi.org/10.1038/nature14236>
- [19] A. Molchanov, T. Chen, W. Hönig, J. A. Preiss, N. Ayanian, and G. S. Sukhatme, “Sim-to-(multi)-real: Transfer of low-level robust control policies to multiple quadrotors,” *CoRR*, vol. abs/1903.04628, 2019.
- [20] J. Panerati, H. Zheng, S. Zhou, J. Xu, A. Prorok, and A. P. Schoellig, “Learning to fly—a gym environment with pybullet physics for reinforcement learning of multi-agent quadcopter control,” in *2021 IEEE/RSJ International Conference on Intelligent Robots and Systems (IROS)*, 2021.

- [21] X. B. Peng, M. Andrychowicz, W. Zaremba, and P. Abbeel, “Sim-to-real transfer of robotic control with dynamics randomization,” in *2018 IEEE International Conference on Robotics and Automation (ICRA)*, 2018, pp. 3803–3810.
- [22] J. Schulman, S. Levine, P. Abbeel, M. Jordan, and P. Moritz, “Trust region policy optimization,” in *Proceedings of the 32nd International Conference on Machine Learning*, vol. 37. PMLR, 2015, pp. 1889–1897.
- [23] J. Schulman, P. Moritz, S. Levine, M. Jordan, and P. Abbeel, “High-dimensional continuous control using generalized advantage estimation,” in *Proceedings of the International Conference on Learning Representations*, 2016.
- [24] J. Schulman, F. Wolski, P. Dhariwal, A. Radford, and O. Klimov, “Proximal policy optimization algorithms,” *CoRR*, vol. abs/1707.06347, 2017.
- [25] T. Seyde, I. Gilitschenski, W. Schwarting, B. Stellato, M. Riedmiller, M. Wulfmeier, and D. Rus, “Is bang-bang control all you need? solving continuous control with bernoulli policies,” in *Thirty-Fifth Conference on Neural Information Processing Systems*, 2021.
- [26] D. Silver, T. Hubert, J. Schrittwieser, I. Antonoglou, M. Lai, A. Guez, M. Lanctot, L. Sifre, D. Kumaran, T. Graepel, T. Lillicrap, K. Simonyan, and D. Hassabis, “A general reinforcement learning algorithm that masters chess, shogi, and go through self-play,” *Science*, vol. 362, no. 6419, pp. 1140–1144, 2021/12/10 2018.
- [27] J. Swisher, P. Hyden, S. Jacobson, and L. Schruben, “A survey of simulation optimization techniques and procedures,” in *2000 Winter Simulation Conference Proceedings (Cat. No.00CH37165)*, vol. 1, 2000, pp. 119–128 vol.1.
- [28] J. Tobin, R. Fong, A. Ray, J. Schneider, W. Zaremba, and P. Abbeel, “Domain randomization for transferring deep neural networks from simulation to the real world,” in *2017 IEEE/RSJ International Conference on Intelligent Robots and Systems (IROS)*, 2017, pp. 23–30.
- [29] O. Vinyals, I. Babuschkin, W. M. Czarnecki, M. Mathieu, A. Dudzik, J. Chung, D. H. Choi, R. Powell, T. Ewalds, P. Georgiev, J. Oh, D. Horgan, M. Kroiss, I. Danihelka, A. Huang, L. Sifre, T. Cai, J. P. Agapiou, M. Jaderberg, A. S. Vezhnevets, R. Leblond, T. Pohlen, V. Dalibard, D. Budden, Y. Sulsky, J. Molloy, T. L. Paine, C. Gulcehre, Z. Wang, T. Pfaff, Y. Wu, R. Ring, D. Yogatama, D. Wünsch, K. McKinney, O. Smith, T. Schaul, T. Lillicrap, K. Kavukcuoglu, D. Hassabis, C. Apps, and D. Silver, “Grandmaster level in starcraft ii using multi-agent reinforcement learning,” *Nature*, vol. 575, no. 7782, pp. 350–354, 2019.

APPENDIX

Table 2: Drone parameters.

Parameter	Value	Physical Unit
Gravitational acceleration g	9.81	m/s
Inertial I_{xx}	$1.33 \cdot 10^{-5}$	kg m ²
Inertial I_{yy}	$1.33 \cdot 10^{-5}$	kg m ²
Inertial I_{zz}	$2.64 \cdot 10^{-5}$	kg m ²
Mass	0.028	kg
Thrust-to-weight ratio k_F	1.8	N/kg
Torque-to-weight ratio k_{M_1}	$5.96 \cdot 10^{-3}$	Nm/N
Torque-to-weight ratio k_{M_2}	$1.56 \cdot 10^{-5}$	Nm

Table 3: Algorithm hyper-parameters used in all experiments. The values marked with * are determined through grid searches while values marked with # depend on environment specifics (see Sect. 5).

Hyper-parameter	PPO
Actor learning rate	0.0003
Actor mini-batch size	1000
Actor mini-batch updates	80
Actor network	(50,50, ReLU)
Actor optimizer	Adam
Batch-size of roll-outs	64,000
Clipping factor	0.2
Critic learning rate	0.001
Critic mini-batch size	62
Critic mini-batch updates	80
Critic network	(64,64, tanh)
Critic optimizer	Adam
Discount factor γ	0.99
Distributed learners	64
Entropy co-efficient	0
Exploration noise ϵ (linearly annealed)	0.5 \rightarrow 0.001
GAE factor λ	0.95
Maximal Trajectory Length	500
Training Epochs	500
Weight initialization gain	$\sqrt{5}$
Weight initialization	Kaiming Uniform